Symmetry as a Continuous Feature

Hagit Zabrodsky, Shmuel Peleg, and David Avnir

Abstract—Symmetry is treated as a continuous feature and a Continuous Measure of Distance from Symmetry in shapes is defined. The Symmetry Distance (SD) of a shape is defined to be the minimum mean squared distance required to move points of the original shape in order to obtain a symmetrical shape. This general definition of a symmetry measure enables a comparison of the "amount" of symmetry of different shapes and the "amount" of different symmetries of a single shape. This measure is applicable to any type of symmetry in any dimension. The Symmetry Distance gives rise to a method of reconstructing symmetry of occluded shapes. We extend the method to deal with symmetries of noisy and fuzzy data. Finally, we consider grayscale images as 3D shapes, and use the Symmetry Distance to find the orientation of symmetric objects from their images, and to find locally symmetric regions in images.

Index Terms—Symmetry, local symmetry, symmetry distance, similarity measure, occlusion, fuzzy shapes, face orientation.

I. INTRODUCTION

ONE of the basic features of shapes and objects is symmetry. Symmetry is considered a pre-attentive feature which enhances recognition and reconstruction of shapes and objects [4]. Symmetry is also an important parameter in physical and chemical processes and is an important criterion in medical diagnosis.

However, the exact mathematical definition of symmetry [23], [32] is inadequate to describe and quantify the symmetries found in the natural world nor those found in the visual world (a classic example is that of faces—see Fig. 1). Furthermore, even perfectly symmetric objects lose their exact symmetry when projected onto the image plane or the retina due to occlusion, perspective transformations, digitization, etc. Thus, although symmetry is usually considered a binary feature, (i.e., an object is either symmetric or it is not symmetric), we view symmetry as a continuous feature where intermediate values of symmetry denote some intermediate "amount" of symmetry. This concept of continuous symmetry is in accord with our perception of symmetry as can be seen, for example, in Fig. 2

Considering symmetry as a continuous feature, we introduce a "Symmetry Distance" that can measure and quantify all types of symmetries of objects. This measure will enable a comparison of the "amount" of symmetry of different shapes and the "amount" of different symmetries of a single shape. Additionally, we present a simple and general algorithm for evaluating this measure.
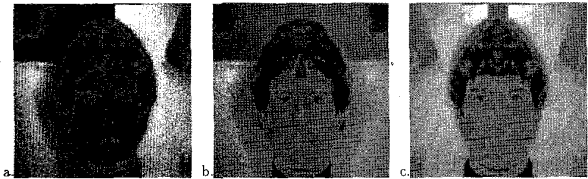
Fig. 1. Faces are not perfectly symmetrical. a) original image; b) left half of original image and its reflection; c) right half of original image and its reflection.
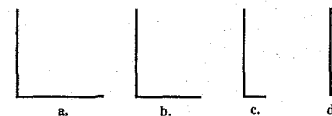

Fig. 2. Perceiving continuous symmetry. a) a shape perceived as perfectly symmetric (the oblique mirror axis passing through the vertex; b) shortening an arm, the shape is perceived as "almost" symmetric; c) further shortening of the arm, the shape is perceived as having "less" symmetry; d) when the arm is eliminated, the shape is again perfectly symmetric (with a mirror axis perpendicular to the existing arm).

We define the Symmetry Distance in Section II, and we describe a method for evaluating this measure in Section III. In Sections IV-VI, we describe features of the symmetry distance, including its use in dealing with occluded objects and noisy data. Finally, in Section VII, we describe the application of the symmetry distance to finding face orientation and locally symmetric regions in images.

A. Definitions of Symmetry

In this paper, we refer to the symmetries defined below, although the definitions, methods and discussions presented in this work apply to all other symmetries in any dimension. For further details and a review see [34].

A 2D object is **mirror-symmetric** if it is invariant under a reflection about a line (the mirror-symmetry axis).

A 3D object is **mirror-symmetric** if it is invariant under a reflection about a plane.

A 2D object has **rotational-symmetry** of order n, denoted C_n-**Symmetry**, if it is invariant under rotation of $\frac{2\pi}{n}$ radians about the center of mass of the object.

A 3D object has **rotational-symmetry** of order n, denoted C_n-**Symmetry**, if it is invariant under rotation of $\frac{2\pi}{n}$ radians about a line (the rotational symmetry axis) passing through the center of mass of the object.

Radial symmetry is the symmetry of a 2D object having both mirror-symmetry and C_n-symmetry (note that such objects have n axes of mirror-symmetry). Radial symmetry of order n is denoted D_n-**Symmetry**. Circular symmetry is C_∞-symmetry (see Fig. 3).
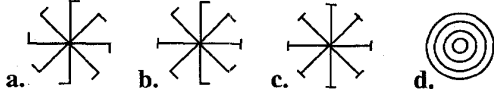
Fig. 3. Examples of symmetries: a) C_8-symmetry; b) mirror-symmetry; c) D_8-symmetry; d) circular symmetry.

B. Studies of Symmetry In Computer Vision

Detection of symmetry in images has been widely studied; with respect to circular (radial) symmetries [6], [29] and with respect to mirror symmetries [22], [26]. Transformation of the symmetry detection problem to a pattern matching problem introduces efficient algorithms for detection of mirror and rotational symmetries and the location of symmetry axes [3], [1]. These algorithms assume noise free input and detect symmetry, if exists, on a global scale.

As an intrinsic characteristic of objects and shapes, symmetry has been used to describe and recognize shapes and objects both on a global scale [17], [21] and as a local feature [10], [8], [28]. Symmetrical features of images have been exploited for better image compression [20]. Symmetrical descriptions of shapes and the detection of symmetrical features of objects are useful in guiding shape matching, model-based object matching and object recognition [27], [29]. Reconstruction of 3D objects has also been implemented using symmetry as a constraint [31], [24]. More recently, symmetry has been used to discriminate textures [9] and has been used in guiding robot grasping [7].

Considerable work has been done on skewed symmetries including detection and exploiting them in the reconstruction of 3D structure [26], [27], [18], [14], [28].

So far, symmetry has been treated as a binary feature: either it exists or it does not exist. The approach to symmetry as a continuous feature is novel, although several early studies have approached the question of measuring symmetry: In an early work, Grünbaum [15] reviews methods of geometrically measuring symmetry of convex sets. Yodogawa [33] has presented an evaluation of symmetry (namely "Symmetropy") in single patterns which uses information theory to evaluate the distribution of symmetries in a pattern. Marola [22] presents a coefficient of mirror-symmetry with respect to a given axis where global mirror-symmetry is found by roughly estimating the axis location and then fine tuning the location by minimizing the symmetry coefficient. Gilat [13], Hel-Or, Peleg, and Avnir [16], and Avnir and Meyer [5] present the idea of a *Measure of Chirality* (a measure of deviation from mirror-symmetry). Similar to Marola, Gilat's chirality measure is based on minimizing the volume difference between the object and it's reflection through a varying plane of reflection. Hel-Or et al. present a measure of chirality for 2D objects based on rotational effects of chiral bodies on the surround.

These symmetry detection and evaluation methods are each limited to a certain type of symmetry (mirror or circular symmetry). In this paper we introduce the notion of continuous symmetry and present a general continuous measure the *symmetry distance* for evaluating all types of symmetries in any dimension.

II. A CONTINUOUS SYMMETRY MEASURE—DEFINITION

We define the **Symmetry Distance** (SD) as a quantifier of the minimum 'effort' required to transform a given shape into a symmetric shape. This 'effort' is measured by the mean of the square distances each point is moved from its location in the original shape to its location in the symmetric shape. Note that no a priori symmetric reference shape is assumed.

Denote by Ω the space of all shapes of a given dimension, where each shape P is represented by a sequence of n points $\{P_i\}_{i=0}^{n-1}$. We define a metric d on this space as follows:

$$d : \Omega \times \Omega \to R$$

$$d(P,Q) = d(\{P_i\},\{Q_i\}) = \frac{1}{n}\sum_{i=0}^{n-1}\|P_i - Q_i\|^2$$

this metric defines a distance function between every two shapes in Ω.

We define the **Symmetry Transform** of a shape P as the symmetric shape $\hat{P}$, closest to P in terms of metric d.

The **Symmetry Distance (SD)** of a shape P is defined as the distance between P and it's Symmetry Transform:

$$SD = d(P, \hat{P})$$

The SD of a shape $P = \{P_i\}_{i=0}^{n-1}$ is evaluated by finding the symmetry transform $\hat{P}$ of P and computing:

$$SD = \frac{1}{n}\sum_{i=0}^{n-1}\|P_i - \hat{P}_i\|^2$$

This definition of the Symmetry Distance implicitly implies invariance to rotation and translation. Normalization of the original shape prior to the transformation additionally allows invariance to scale (Fig. 4). We normalize by scaling the shape so that the maximum distance between points on the contour and the centroid is a given constant (in this paper all examples are given following normalization to 10). The normalization presents an upper bound on the mean squared distance moved by points of the shape. Thus the SD value is limited in range, where SD = 0 for perfectly symmetric shapes. The general definition of the Symmetry Distance enables evaluation of a given shape for different types of symmetries (mirror-symmetries, rotational symmetries etc.). Moreover, this generalization allows comparisons between the different symmetry types, and allows expressions such as "a shape is more mirror-symmetric than C_2-symmetric."

An additional feature of the Symmetry Distance is that we obtain the symmetric shape which is 'closest' to the given one, enabling visual evaluation of the SD.

An example of a 2D polygon and it's symmetry transforms and SD values are shown in Fig. 5. Note that the shape in Fig. 5e is the most similar to the original shape Fig. 5a and, indeed, its SD value is the smallest. In the next section, we describe a geometric algorithm for deriving the Symmetry Transform of a shape. In Section IV, we deal with the initial step of representing a shape by a collection of points.
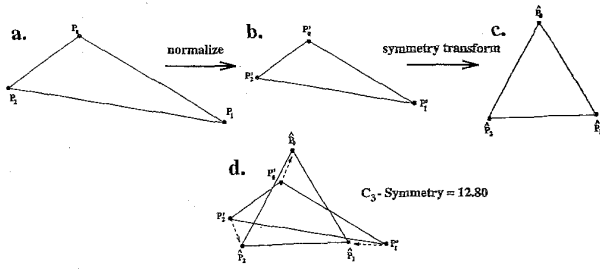
Fig. 4. Calculating the symmetry distance of a shape: a) original shape $\{P_0,\ P_1,\ P_2\}$; b) normalized shape $\{P_0',\ P_1',\ P_2'\}$, such that maximum distance to the center of mass is a given constant (10); c) applying the symmetry transform to obtain a symmetric shape $\{\hat{P}_0, \hat{P}_1, \hat{P}_2\}$; d) SD $= \frac{1}{3}\left(\left\|P_0' - \hat{P}_0\right\|^2 + \left\|P_1' - \hat{P}_1\right\|^2 + \left\|P_2' - \hat{P}_2\right\|^2\right)$.
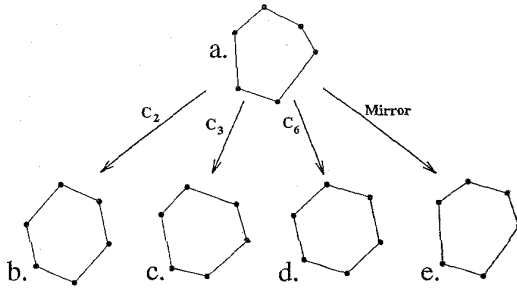

Fig. 5. Symmetry transforms of a 2D polygon. a) 2D polygon and its symmetry transform with respect to: b) C_2-symmetry (SD = 1.87); c) C_3-symmetry (SD = 1.64); d) C_6-symmetry (SD = 2.53); e) mirror-symmetry (SD = 0.66).

III. EVALUATING THE SYMMETRY TRANSFORM

In this Section, we describe a geometric algorithm for deriving the Symmetry Transform of a shape represented by a sequence of points $\{P_i\}_{i=0}^{n-1}$. In practice we find the Symmetry Transform of the shape with respect to a given symmetry group. For simplicity and clarity of explanation, we describe the method by using some examples. Mathematical proofs and derivations can be found in Appendix A.

We first present the algorithm for C_n-symmetry and later generalize it to any finite symmetry group.

Following is a geometrical algorithm for deriving the symmetry transform of a shape P having n points with respect to rotational symmetry of order n (C_n-symmetry). This method transforms P into a regular n-gon, keeping the centroid in place.

Algorithm for finding the C_n-symmetry transform:

1) *Fold* the points $\{P_i\}_{i=0}^{n-1}$ by rotating each point P_i counterclockwise about the centroid by $2\pi i/n$ radians (Fig. 6b).

2) Let $\hat{P}_0$ be the average of the points $\{\widetilde{P}_i\}_{i=0}^{n-1}$ (Fig. 6c).

3) *Unfold* the points, obtaining the C_n-symmetric points

$\{\hat{P}_i\}_{i=0}^{n-1}$ by duplicating $\hat{P}_0$ and rotating clockwise about the centroid by $2\pi i/n$ radians (Fig. 6d).
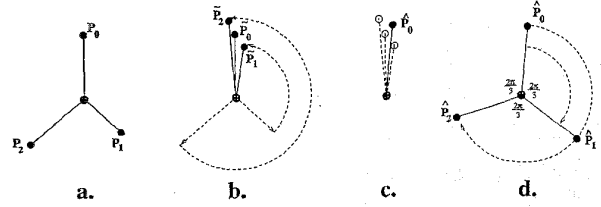

Fig. 6. The C_3-symmetry transform of three points. a) original three points $\{P_i\}_{i=0}^{2}$; b) fold $\{P_i\}_{i=0}^{2}$ into $\{\widetilde{P}_i\}_{i=0}^{2}$; c) average $\{\widetilde{P}_i\}_{i=0}^{2}$ obtaining $\hat{P}_0 = \frac{1}{3}\sum_{i=0}^{2}\widetilde{P}_i$; d) unfold the average points obtaining $\{\hat{P}_i\}_{i=0}^{2}$. The centroid ω is marked by $\oplus$.

The set of points $\{\hat{P}_i\}_{i=0}^{n-1}$ is the symmetry transform of the points $\{P_i\}_{i=0}^{n-1}$; i.e., they are the C_n-symmetric configuration of points closest to $\{P_i\}_{i=0}^{n-1}$ in terms of the metric d defined in Section II (in terms of the average distance squared). Proof is given in Appendix A.

The common case, however, is that shapes have more points than the order of the symmetry. For symmetry of order n, the folding method can be extended to shapes having a number of points which is a multiple of n. A 2D shape P having qn points is represented as q sets $\{S_r\}_{r=0}^{q-1}$ of n interlaced points $S_r = \{P_{iq+r}\}_{i=0}^{n-1}$ (see discussion in Appendix C). The C_n-symmetry transform of P (Fig. 7) is obtained by applying the above algorithm to each set of n points seperately, where the folding is performed about the centroid of all the points.
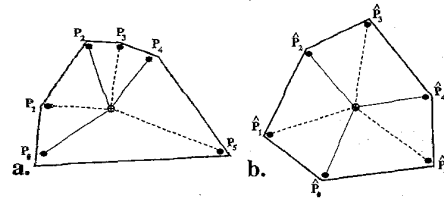

Fig. 7. Geometric description of the C_3-symmetry transform for six points. The centroid ω of the points is marked by $\oplus$. a) the original points shown as two sets of three points: $S_0 = \{P_0, P_2, P_4\}$ and $S_1 = \{P_1, P_3, P_5\}$; b) the obtained C_3-symmetric configuration.

The procedure for evaluating the symmetry transform for mirror-symmetry is similar: Given a shape having $m = 2q$ points we divide the points into q pairs of points (see Appendix C) and given an initial guess of the symmetry axis, we apply the folding/unfolding method as follows (see Fig. 8):

Algorithm for finding the mirror-symmetry transform:

1) for every pair of points $\{P_0, P_1\}$:

   a) fold—by reflecting across the mirror symmetry axis obtaining $\{\widetilde{P}_0, \widetilde{P}_1\}$.

   b) average—obtaining a single averaged point $\hat{P}_0$.

   c) unfold—by reflecting back across the mirror symmetry axis obtaining $\{\hat{P}_0, \hat{P}_1\}$.

2) minimize over all possible axes of mirror-symmetry.

The minimization performed in step 2 is, in practice, replaced by an analytic solution (see Appendix B).
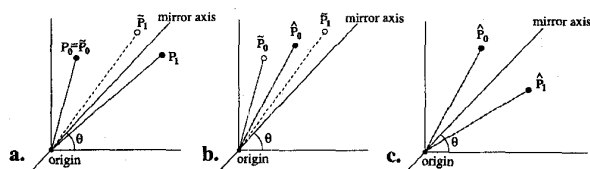

Fig. 8. The mirror-symmetry transform of a single pair of points for angle θ, where the centroid of the shape is assumed to be at the origin; a) the two points $\{P_0, P_1\}$ are folded to obtain $\{\widetilde{P}_0, \widetilde{P}_1\}$; b) points $\widetilde{P}_0$ and $\widetilde{P}_1$ are averaged to obtain $\hat{P}_0$; c) $\hat{P}_1$ is obtained by reflecting $\hat{P}_0$ about the symmetry axis.

This method extends to **any** finite point-symmetry group G in **any** dimension, where the folding and unfolding are performed by applying the group elements about the centroid (see derivations in Appendix A):

Given a finite symmetry group G (having n elements) and given a shape P represented by $m = qn$ points, the symmetry transform of the shape with respect to G-symmetry is obtained as follows:

Algorithm for finding the G-symmetry transform:

1) The points are divided into q sets of n points.

2) For every set of n points:

   a) The points are folded by applying the elements of the G-symmetry group.

   b) The folded points are averaged, obtaining a single averaged point.

   c) The averaged point is unfolded by applying the inverse of the elements of the G-symmetry group. A G-symmetric set of n points is obtained.

3) The above procedure is performed over all possible orientations of the symmetry axis and planes of G. Select that orientation which minimizes the Symmetry Distance value. As previously noted, this minimization is analytic in 2D (derivation is given in Appendix B) but requires an iterative minimization process in 3D (except for the 3D mirror-symmetry group where a closed form solution has been derived—see [35]).

Thus, the Symmetry Distance of a shape may be evaluated with respect to any finite symmetry group. One may consider as the 'appropriate' symmetry of a shape, that symmetry group which minimizes the Symmetry Distance. A minimization over

all symmetry groups can be applied, however, minimization over a finite number of low order groups usually suffices (in 2D minimization over mirror and prime-ordered rotational symmetries is sufficient. Since evaluation of the Symmetry Distance in 2D is analytical, this minimization is inexpensive).

IV. POINT SELECTION FOR SHAPE REPRESENTATION

As symmetry has been defined on a sequence of points, representing a given shape by points must precede the application of the symmetry transform. Selection of points influences the value of SD and depends on the type of object to be measured. If a shape is inherently created from points (such as a graph structure or cyclically connected points creating a polygon) we can represent a shape by these points (Fig. 9). This is the case when analysing symmetry of molecules ([37], [35]). There are several ways to select a sequence of points to represent continuous 2D shapes. One such method is selection at equal distances - the points are selected along the shape's contour such that the curve length between every pair of adjacent points is equal (Fig. 10).
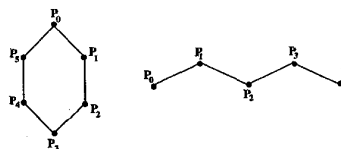

Fig. 9. When measuring symmetry of shapes inherently created from points, we represent the shape by these points.
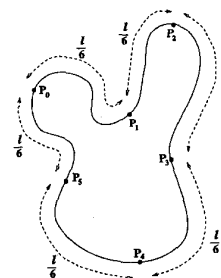

Fig. 10. Point selection by equal distance: points are selected along the contour at equal distances in terms of curve length. In this example, six points are distributed along the contour spaced by $\frac{1}{6}$ of the full contour length.

In many cases, however, contour length is not a meaningful measure, as in noisy or occluded shapes. In such cases we propose to select points on a smoothed version of the contour and then project them back onto the original contour.

The smoothing of the continuous contour is performed by moving each point on the continuous contour to the centroid of its contour neighborhood. The greater the size of the neighborhood, the greater is the smoothing (see Fig. 11). The level of smoothing can vary and for a high level of smoothing, the resulting shape becomes almost a circle about the centroid

[25]. In this case, equal distances on the circular contour is equivalent to equal angles about the center. For maximum smoothing we, therefore, use selection at **equal angles** (Fig. 12) where points are selected on the original contour at equal angular intervals around the centroid. For further details on the selection of points by smoothing see [34].
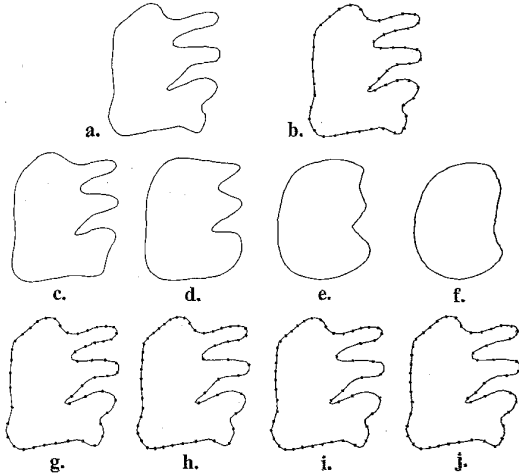

Fig. 11. Selection by smoothing. a) original continuous contour; b) points are selected at equal distances along the contour; c)-f) the smoothed shape is obtained by averaging neighboring points of b). (The amount of smoothing depends on the size of the neighborhood. The smoothed shapes (c-f) are obtained when the neighborhood includes 5, 10, 15, and 20% of the points, respectively); g)-j) the sampling of points on the original shape using the smoothed shapes (c-f), respectively. (Notice that fewer points are selected on the "noisy" part of the contour.)
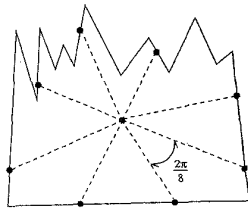

Fig. 12. Selection at equal angles: points are distributed along the contour at regular angular intervals around the centroid.

V. Symmetry of Occluded Shapes —Center of Symmetry

As described in Section IV, a shape can be represented by points selected at regular angular intervals about the centroid. Angular selection of points about a point other than the centroid will give a different symmetry distance value. We define the **center of symmetry** of a shape as that point in the 2D plane about which selection at equal angles gives the minimum symmetry distance value (Fig. 13). Intuitively, the center of symmetry is that point about which rotation of the shape aligns it as close as possible with itself (in terms of the mean squared distances). When a symmetric shape is complete the center of symmetry coincides with the centroid of the shape. However,

the center of symmetry of truncated or occluded objects does not align with its centroid but is closer to the centroid of the complete shape. Thus the center of symmetry of a shape is robust under truncation and occlusion.
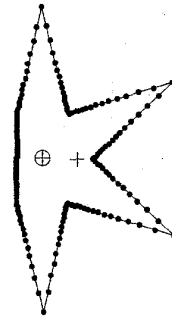

Fig. 13. An occluded shape with sampled points selected at equal angles about the center of symmetry (marked by ⊕). The symmetry distance obtained using these points is smaller than the symmetry distance obtained using points selected at equal angles about the centroid (marked by +).

To locate the center of symmetry, we use an iterative procedure of gradient descent that converges from the centroid of an occluded shape to the center of symmetry. Denote by *center of selection*, that point about which points are selected using selection at equal angles. We initialize the iterative process by setting the centroid as the center of selection. At each step we compare the symmetry value obtained from points selected at equal angles about the center of selection with the symmetry value obtained by selection about points in the center of selection's immediate neighborhood. That point about which selection at equal angles gives minimum symmetry value, is set to be the new center of selection. If the center of selection does not change, the neighborhood size is decreased. The process is terminated when neighborhood size reaches a predefined minimum size. The center of selection at the end of the process is taken as the center of symmetry.

In the case of occlusions (Fig. 14), the closest symmetric shape obtained by angular selection about the center of symmetry is visually more similar to the original than that obtained by angular selection about the centroid. We can reconstruct the symmetric shape closest to the unoccluded shape by obtaining the symmetry transform of the occluded shape using angular selection about the center of symmetry (see Fig. 14c). In Fig. 15, the center of symmetry and the closest symmetric shapes were found for several occluded flowers.
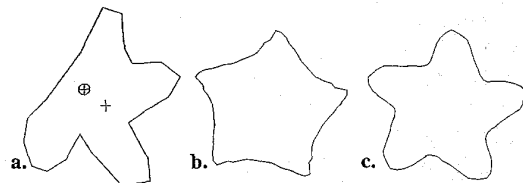

Fig. 14. Reconstruction of an occluded shape. a) original occluded shape, its centroid (+) and its center of symmetry (⊕); b)-c) the closest C_5-symmetric shape using angular selection about the centroid b) and about the center of symmetry c). (Selection about the centroid gives a featureless shape, while selection about the center of symmetry yields a more meaningful shape.)
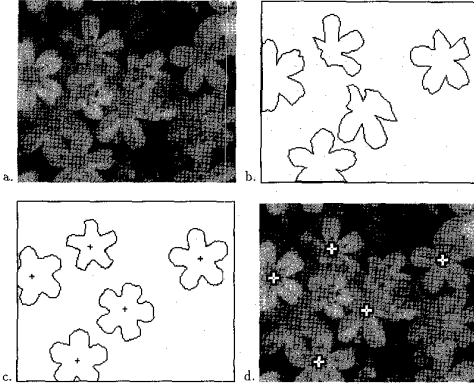
Fig. 15. Reconstruction of occluded objects. a) a collection of occluded asymmetric flowers; b) contours of the occluded flowers were extracted manually; c) the closest symmetric shapes and their center of symmetry; d) the center of symmetry of the occluded flowers is marked by '+'.

The process of reconstructing the occluded shape can be improved by altering the method of evaluating the symmetry of a set of points. As described in Section III, the symmetry of a set of points is evaluated by folding, averaging and unfolding about the centroid of the points. We alter the method as follows:

1) The folding and unfolding (steps 1 and 3) will be performed about the center of symmetry rather than about the centroid of the points.

2) Rather than averaging the folded points (step 2), we apply other robust clustering methods. In practice we average over the folded points, drop the points farthest from the average and then reaverage (see Fig. 16).
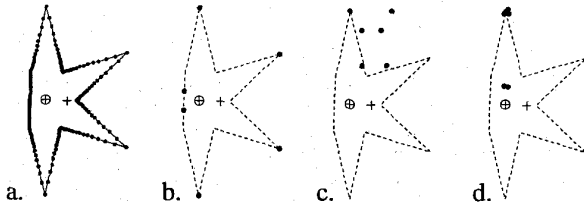

Fig. 16. Improving the averaging of folded points. a) an occluded shape with points selected using angular selection about the center of symmetry (marked as ⊕); b) a single set (orbit) of the selected points of a) is shown; c) folding the points about the centroid (marked by +), points are clustered sparsely; d) folding the points about the center of symmetry, points are clustered tightly. (Eliminating the extremes (two farthest points) and averaging results in a smaller averaging error and better reconstruction.)

Intuitively, the robust clustering causes the reconstruction to be strongly influenced by contour points on the unoccluded portion of the shape while eliminating the influence of the points on the contour representing the truncated or occluded portion of the shape.

The improvement in reconstruction of an occluded shape is shown in Fig. 17. This method improves both shape and localization of the reconstruction. Assuming that the original shape was symmetric, this method can reconstruct an occluded shape very accurately.
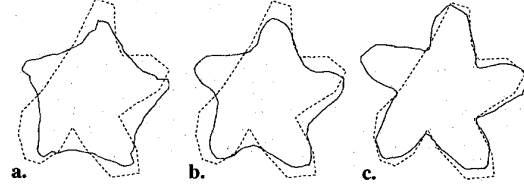

Fig. 17. Improving the reconstruction. The original shape is shown as a dashed line and the reconstructed shape as a solid line. a) the closest symmetric shape using angular selection about the centroid; b) the closest symmetric shape using angular selection about the center of symmetry; c) the closest symmetric shape using angular selection about the center of symmetry and the robust clustering.

VI. SYMMETRY OF POINTS WITH UNCERTAIN LOCATIONS

In most cases, sensing processes do not have absolute accuracy and the location of each point in a sensed pattern can be given only as a probability distribution. Given sensed points with such uncertain locations, the following properties are of interest:

- The most probable symmetric configuration represented by the sensed points.
- The probability distribution of symmetry distance values for the sensed points.

A. The Most Probable Symmetric Shape

Fig. 18a shows a configuration of points whose locations are given by a normal distribution function. The dot represents the expected location of the point and the rectangle represents the standard deviation marked as rectangles having width and length proportional to the standard deviation. In this section we briefly describe a method of evaluating the most probable symmetric shape under the Maximum Likelihood criterion [12] for a given set of measured points (measurements). Detailed derivations and proofs are given in [38]. For simplicity we describe the method with respect to C_n-symmetry. The solution for mirror symmetry or any other symmetry is similar (see [38]).
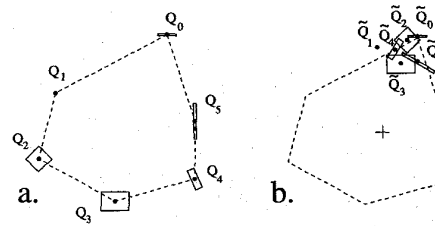
Fig. 18. Folding measured points. a) a configuration of six measured points $Q_0 \cdots Q_5$ (The dot represents the expected location of the point. The rectangle represents the standard deviation marked as rectangles having width and length proportional to the standard deviation.); b) each measured point Q_i was rotated by $2\pi i/6$ radians about the centroid of the expected point locations (marked as '+') obtaining $\tilde{Q}_0 \ldots \tilde{Q}_5$.

Given n ordered points in 2D whose locations are given as normal probability distributions with expected location P_i and

covariance matrix Λ_i: $Q_i \sim \mathcal{N}(P_i, \Lambda_i)$, $i = 0 \ldots n - 1$, we find the C_n-symmetric configuration of points at locations $\left\{ \hat{P}_i \right\}_0^{n-1}$, which is optimal under the Maximum Likelihood criterion [12].

Denote by ω the centeroid of the most probable C_n-symmetric set of locations $\hat{P}_i$:

$$\omega = \frac{1}{n} \sum_{i=0}^{n-1} \hat{P}_i .$$

The point ω is dependent on the location of the measurements (P_i) and on the probability distribution associated with them (Λ_i). Intuitively, ω is positioned at that point about which the folding (described below) gives the tightest cluster of points with small uncertainty (small s.t.d.). We assume for the moment that ω is given (a method for finding ω is derived in [38]). We use a variant of the folding method which was described in Section III for evaluating C_n-symmetry of a set of points:

1) The n measurements $Q_i \sim \mathcal{N}(P_i, \Lambda_i)$ are *folded* by rotating each measurement Q_i by $2\pi i / n$ radians about the point ω. A new set of measurements $\tilde{Q}_i \sim \mathcal{N}\left(\tilde{P}_i, \tilde{\Lambda}_i\right)$ is obtained (see Fig. 18b).

2) The folded measurements are *averaged* using a weighted average, obtaining a single point $\hat{P}_0$. Averaging is done by considering the n folded measurements $\tilde{Q}_i$ as n measurements of a single point and $\hat{P}_0$ represents the most probable location of that point under the Maximum Likelihood criterion.

$$\hat{P}_0 - \omega = \left(\sum_{j=0}^{n-1} \tilde{\Lambda}_j^{-1} \right)^{-1} \sum_{i=0}^{n-1} \tilde{\Lambda}_i^{-1} \tilde{P}_i - \omega$$

3) The "average" point $\hat{P}_0$ is *unfolded* as described in Section III obtaining points $\left\{ \hat{P}_i \right\}_{i=0}^{n-1}$, which are perfectly C_n-symmetric.

When we are given $m = qn$ measurements, we find the most probable C_n-symmetric configuration of points, similar to the folding method of Section III. The m measurements $\left\{ Q_i \right\}_{i=0}^{m-1}$, are divided into q interlaced sets of n measurements each, and the folding method as described above is applied seperately to each set of measurements. Derivations and proof of this case is also found in [38].

Several examples are shown in Fig. 19, where for a given set of measurements, the most probable symmetric shapes were found. Fig. 20 shows an example of varying the probability distribution of the measurements on the resulting symmetric shape.

B. The Probability Distribution of Symmetry Values

Fig. 21a displays a Laue photograph [2] which is an intereference pattern created by projecting X-ray beams onto crystals. Crystal quality is determined by evaluating the symmetry of the pattern. In this case, the interesting feature is not the closest symmetric configuration, but the probability distribution of the symmetry distance values.
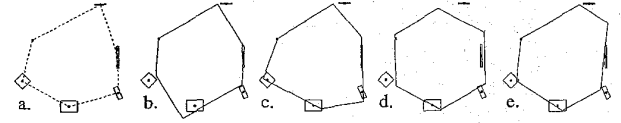

Fig. 19. The most probable symmetric shape. a) a configuration of six measured points; b)-e) the most probable symmetric shapes with respect to b) C_2-symmetry; c) C_3-symmetry; d) C_6-symmetry; e) mirror-symmetry.
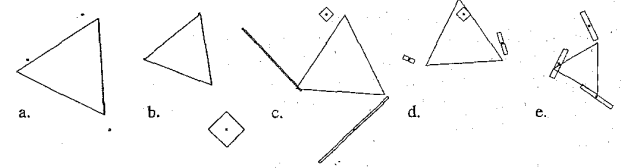

Fig. 20. The most probable C_3-symmetry shape for a set of measurements after varying the probability distribution and expected locations of the measurements. a)-c) changing the uncertainty (s.t.d) of the measurements; d)-e) changing both the uncertainty and the expected location of the measurements.

Consider the configuration of 2D measurements given in Fig. 18a. Each measurement Q_i is a normal probability distribution $Q_i \sim \mathcal{N}(P_i, \Lambda_i)$. We assume the centroid of the expectation of the measurements is at the origin. The probability distribution of the symmetry distance values of the original measurements is equivalent to the probability distribution of the location of the "average" point $\hat{P}_0$ given the folded measurements as obtained in step 1 and step 2 of the algorithm in Section VI.A. It is shown in [38] that this probability distribution is a χ^2 distribution of order $n - 1$. However, we can approximate the distribution by a gaussian distribution. Details of the derivation are given in [38].
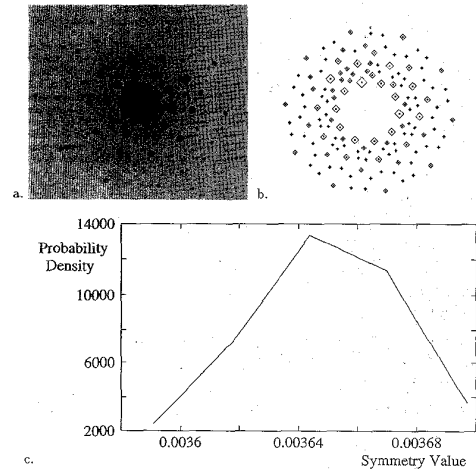
Fig. 21. Probability distribution of symmetry values. a) interference pattern of crystals; b) probability distribution of point locations corresponding to a); c) probability distribution of symmetry distance values with respect to C_{10}-symmetry was evaluated as described in the text. (Expectation value = 0.003663.)

In Fig. 21, we display distributions of the symmetry distance value as obtained for the Laue photograph given in Fig. 21a. In this example we considered every dark patch as a

measured point with variance proportional to the size of the patch. Thus, in Fig. 21b the rectangles which are proportional in size to the corresponding dark patches of Fig. 21a, represent the standard deviation of the locations of point measurements. Note that a different analysis could be used in which the variance of the measurement location is taken as inversely proportional to the size of the dark patch.

In Fig. 22, we display distributions of the symmetry distance value for various measurements. As expected, the distribution of symmetry distance values becomes broader as the uncertainties (the variance of the distribution) of the measurements increase.
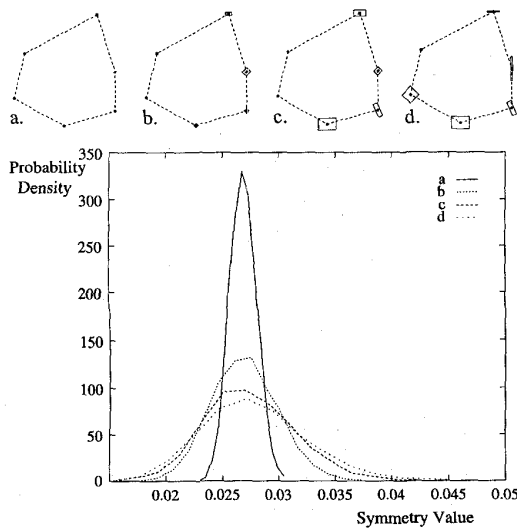

Fig. 22. Probability distribution of the symmetry distance value as a function of the variance of the measured points. a)-d) some examples of configurations of measured points; graph at bottom shows probability distribution of symmetry distance values with respect to C_6-symmetry for the configurations a)-d).

VII. APPLICATION TO IMAGES

A. Finding Orientation of Symmetric 3D Objects

When dealing with images, we let pixel values denote elevation, and consider an image as a 3D object on which we can measure 3D symmetries. We applied the SD to find orientation of symmetric 3D objects by finding their 3D mirror-symmetry. The 3D shape is represented by a set of 3D points: for a possible reflection plane, the plane perpendicular to it is sampled. Each sampled points is projected onto the 3D object and its elevation is recomputed relative to the sampling plane (Fig. 23). The symmetry value for 3D mirror-symmetry is evaluated using the projected sampling points. The final reflection plane of the 3D object is determined by minimizing the symmetry value over all possible reflection planes. In practice only feasible symmetry planes were tested (i.e., planes which intersect the 3D image) and a gradient descent algorithm was used to increase efficiency of convergence to the minimum symmetry value (the SD). Examples are shown in Fig. 24, where a symmetric 3D object is rotated into a frontal

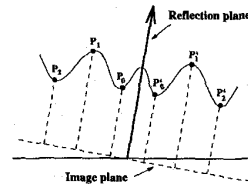vertical view after the reflection plane was found.

Fig. 23. Selecting points on the 3D object (a 2D analog is shown). For a possible reflection plane, the plane perpendicular to it is sampled. Elevations are recomputed on the object relative to the sampling plane.
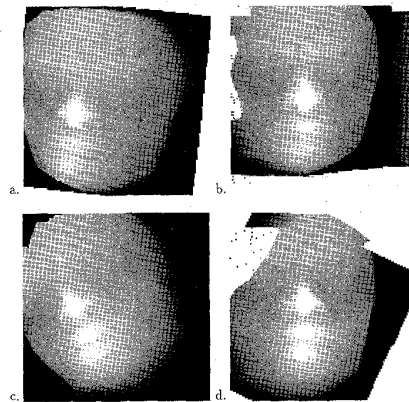

Fig. 24. Applying the SD with respect to 3D mirror-symmetry in order to find orientation of a 3D object. a) and c) original depth maps; b) and d) the symmetry reflection plane has been found and the image rotated to a frontal vertical view.

B. Using a Multiresolution Scheme

In many images the process of finding the reflection plane did not converge to the correct solution, i.e., the process converged to a local minima due to the sensitivity of the symmetry value to noise and digitization errors. To overcome this problem we introduced a multiresolution scheme, where an initial estimation of the symmetry transform is obtained at low resolution (see Fig. 25) and is fine tuned using high resolution images. The solution obtained for the low resolution image is used as an initial guess of the solution for the high resolution image. The low resolution images were obtained by creating gaussian pyramids [11].

C. Finding Locally symmetric Regions

Most images cannot be assumed to have a single global symmetry, but contain a collection of symmetric and almost symmetric patterns (be they objects or background). We aim to locate these local symmetries and segment the symmetrical objects from the background. The following three staged process is used to extract locally symmetric regions in images.

1) The first stage locates *symmetry focals*—those points about which the image is locally symmetric. Several methods can be used to find the symmetry focals ([29],

for example). We used a variant of the multiresolution method presented in [36] for sampling and transmitting an image, which uses a simple model of the human visual attention mechanism.
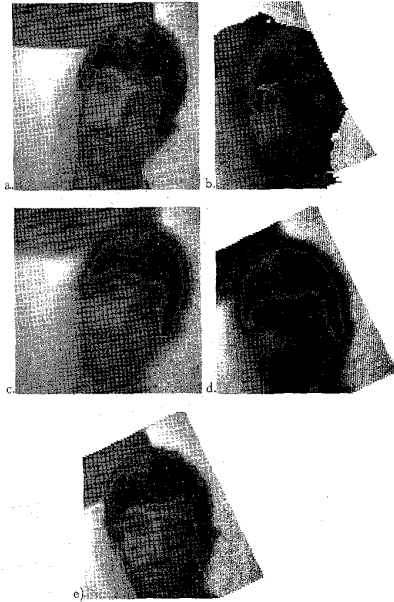

Fig. 25. Using multiresolution to find symmetry. The grey-level image is treated as a depth map and 3D mirror-symmetry is computed. The computed symmetry plane is used to bring the image into a frontal vertical view. a) original image; b) applying the mirror-symmetry transform on a) does not find correct reflection plane; c) a low resolution image obtained by convolving a) with a guassian; d) applying the mirror-symmetry transform on the low resolution image c) give a good estimation of the reflection plane and face orientation; e) using the reflection plane found in d) as an initial guess, the process now converges to the correct symmetry plane.

We used the **Quad Tree** [30] structure which is a hierarchical representation of an image, based on recursive subdivisions of the image array into quadrants.

The process of locating symmetry focals builds a sequence of quad trees and a sequence of corresponding divisions of the image into quadrants. The process is initialized by setting the current quad tree to a single root node (corresponding to the whole image). At each step all quadrants of the image corresponding to the leaves of the quad tree are tested for a given "interest" function. That node of the quad tree that corresponds to the quadrant with highest "interest" value is selected. The current quad tree is expanded by creating the son nodes of the selected node and accordingly, subdividing the image quadrant associated with the selected node. Several steps of this procedure are shown in Fig. 26. In our case the "interest" function was chosen as to be a function of the Symmetry Distance value obtained for the image quadrant. Thus the procedure described focuses onto regions of high symmetry content and finds symmetry focals. In practice, the "interest" function also took into account the busyness of the image quadrant,

thus regions that had low busyness values (i.e., the grey-scale values were almost constant) gave low "interest" values although they were highly symmetric (and gave low Symmetry Distance values). In Fig. 27b, a mirror-symmetry focal and an associated reflection plane (passing through the focal) were found.
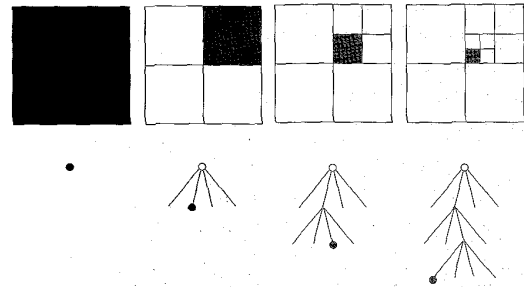

Fig. 26. Several steps in the process of finding symmetry focals. A sequence of quad trees (bottom row) and the corresponding recursive division of the image (top row) is created. The process is initialized by creating a quad tree with a single root node corresponding to the whole image (left). At each step, all quadrants of the image corresponding to the leaves of the quad tree are tested for the "interest" function. The leaf of the quad tree that corresponds to the quadrant with highest value (marked in grey) is expanded to create the quad tree of the next step. Three additional steps are shown.

Fig. 27. Applying the multiresolution scheme to detect a mirror-symmetric region. a) original image; b) a mirror-symmetry focal was found; c) symmetry map of image for the symmetry focal found in b); d) extracted locally symmetric region.

2) Given a symmetry focal and a reflection plane, a symmetry map of the image is created as follows: the original image is sampled at points which are pairwise symmetric with respect to the given reflection plane. The symmetry distance value obtained using the folding method described in Section III for each pair of sampled points is recorded and marked in the symmetry map at the location corresponding to the coordinates of the sampled points. Thus the symmetry map displays the "amount" of mirror-symmetry at every point (with re-

spect to the given reflection plane) where low grey values denote low SD values (i.e., high symmetry content) and high grey values denote high SD values (i.e., low symmetry content) (Fig. 27c).

3) Starting from the symmetry focals, regions are expanded using "active contours" [19] to include compact symmetric regions. The expansion is guided by the symmetry map and continues as long as the pixels included in the locally symmetric region do not degrade the symmetry of the region more than a predefined threshold (Fig. 27d). The process can be continued to extract several locally symmetric regions, as shown in the example of Fig. 28.
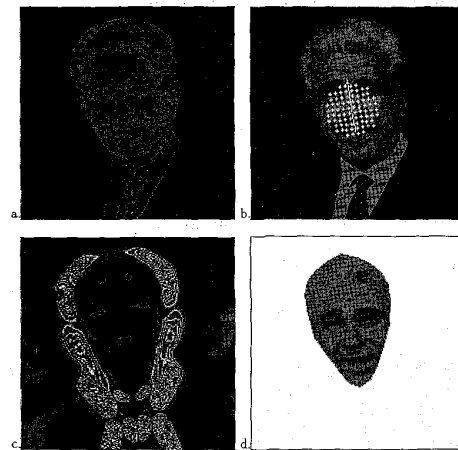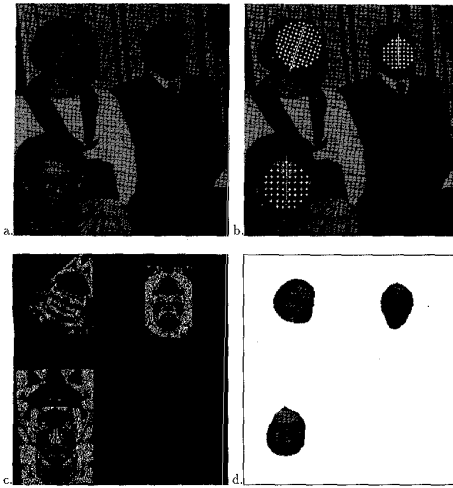

Fig. 28. Applying the multiresolution scheme to find multiple mirror-symmetric regions. a) original image; b) the mirror-symmetry focals found; c) symmetry maps for each mirror-symmetry are merged into a single image; d) extracted locally symmetric regions.

VIII. CONCLUSION

We view symmetry as a continuous feature and define a Symmetry Distance (SD) of shapes. The general definition of the Symmetry Distance enables a comparison of the "amount" of symmetry of different shapes and the "amount" of different symmetries of a single shape. Furthermore, the SD is associated with the symmetric shape which is 'closest' to the given one, enabling visual evaluation of the SD. Several applications were described including reconstruction of occluded shapes, finding face orientation and finding locally symmetric regions in images. We also described how we deal with uncertain data, i.e., with a configuration of measurements representing the probability distribution of point location. The methods described here can be easily extended to higher dimensions and to more complex symmetry groups. Further extensions will deal with other symmetry classes such as planar symmetry (including translatory symmetry and fractals). Additional work has been done on evaluating reflective symmetry (and chirality) of graph structures ([35]). The methods described here have also been extended to deal with skewed and projected

mirror symmetries [39].

APPENDIX A
MATHEMATICAL PROOF OF THE FOLDING METHOD

Given a finite point symmetry group G, we assume without loss of generality that G is centered at the origin (i.e., every element of G leaves the origin fixed). Given an ordering of the n elements of the G-symmetry group $\{g_0 = I, g_1, ..., g_{n-1}\}$ and given n general points $P_0, ..., P_{n-1}$, we find n points $\hat{P}_0, ..., \hat{P}_{n-1}$ and find a rotation matrix R and translation vector w such that the points $\hat{P}_0, ..., \hat{P}_{n-1}$ translated by ω and rotated by R form an ordered orbit under G and bring the following expression to a minimum:

$$\sum_{i=0}^{n-1} \left\| P_i - \hat{P}_i \right\|^2 \tag{1}$$

Since G has a fixed point at the origin and the centroid of the orbit formed by the rotated and translated $\hat{P}_i$ is a fixed point under G, we can assume without loss of generality that the translation vector w is the centroid of points $\hat{P}_i$:

$$w = \frac{1}{n} \sum_{i=0}^{n-1} \hat{P}_i^2 \tag{2}$$

The points $\hat{P}_0, ..., \hat{P}_{n-1}$ translated by ω and rotated by R, form an orbit of G, thus the following must be satisfied:

$$\hat{P}_i = R^t g_i R(\hat{P}_0 - w) + w \quad i = 0 ... n-1 \tag{3}$$

Using Lagrange multipliers with (1)-(3), we minimize the following:

$$\sum_{i=0}^{n-1} \left\| P_i - \hat{P}_i \right\|^2 + \sum_{i=0}^{n-1} \lambda_i^t \left(\hat{P}_i - R^t g_i R(\hat{P}_0 - w) - w \right)$$
$$+ \varepsilon^t \left(w - \frac{1}{n} \sum_{i=0}^{n-1} \hat{P}_i \right) \tag{4}$$

where ε, λ_i for $i = 0 ... n - 1$ are the Lagrange multipliers. Setting the derivatives equal to zero we obtain:

$$\sum_{i=0}^{n-1} \left(P_i - \hat{P}_i \right) = 0$$

and using the last constraint (2) we obtain:

$$w = \frac{1}{n} \sum_{i=0}^{n-1} P_i \tag{5}$$

i.e., the centroid of $P_0, ..., P_{n-1}$ coincides with the centroid of $\hat{P}_0, ..., \hat{P}_{n-1}$ (in terms of the symmetry distance defined in Section I, the centroid of a configuration and the centroid of the closest symmetric configuration is the same for any point symmetry group G).

Noting that $R^t g_i R$ for $i = 0 ... n - 1$ are isometries and distance preserving, we have from the derivatives:

$$\sum_{i=0}^{n-1} R^t g_i^t R\left(P_i - \hat{P}_i\right) = 0$$

Expanding using the constraints we obtain:

$$n\hat{P}_0 - n\omega = \sum_{i=0}^{n-1} R^t g_i^t R P_i - \sum_{i=0}^{n-1} R^t g_i^t R w$$

or

$$\hat{P}_0 - w = \frac{1}{n}\sum_{i=0}^{n-1} R^t g_i^t R(P_i - w) \qquad (6)$$

The derivation of the rotation matrix R is given in the next section, however, given R, the geometric interpretation of (6) is the folding method, as described in Section III, proving that the folding method results in the G-symmetric set of points closest to the given set.

The common case, however, is that shapes have more points than the order of the symmetry. For symmetry of order n, the folding method can be extended to shapes having a number of points which is a multiple of n. Given $m = qn$ points (i.e., q sets of n points) $\left\{P_0^j, ..., P_{n-1}^j\right\} j = 0 \; ...q-1$ we follow the above derivation and obtain a result similar to that given in (6). For each set of n points, i.e., for $j = 0 \; ... \; q - 1$:

$$\hat{P}_0^j - w = \frac{1}{n}\sum_{i=0}^{n-1} R^t g_i^t R\left(P_i^j - w\right) \qquad (7)$$

where

$$w = \frac{1}{m}\sum_{j=0}^{q-1}\sum_{i=0}^{n-1} P_i^j$$

is the centroid of all m points. The geometric interpretation of (7) is the folding method, as described in Section III for the case of a shape represented by $m = qn$ points.

The folding method for the cases where the number of points is not a multiple of the number of elements in G is not derived here. Details of this case can be found in [37].

APPENDIX B
FINDING THE OPTIMAL ORIENTATION IN 2D

The problem of finding the minimizing orientation is irrelevant for the C_n symmetry groups since every element g of these groups is a rotation and $R^t g R = g$. In the case of C_n-symmetry groups, R is usually taken as I (the identity matrix). We derive here a solution for the orientation in the case where G is a D_n symmetry group.

The $2n$ elements of the D_n-symmetry group can be described as the n elements

$$g_0 = I, \; g_1 = R_n^1, \; g_2 = R_n^2, \; ..., \; g_{n-1} = R_n^{n-1}$$

(where R_n^i is the rotation of $2\pi i/n$ radians about the origin) and the n elements obtained by applying a reflection R_f on each of these elements:

$$g_n = R_f, g_{n+1} = R_f R_n^1, \; g_{n+2} = R_f R_n^2, \; ..., \; g_{2n-1} = R_f R_n^{n-1}.$$

We denote the orientation of the symmetry group as the angle θ between the reflection axis and the y axis. Thus

$$R = \begin{pmatrix} \cos\theta & \sin\theta \\ -\sin\theta & \cos\theta \end{pmatrix}$$

and the reflection operation R_f is given by:

$$R_f = \begin{pmatrix} \cos\theta & -\sin\theta \\ \sin\theta & \cos\theta \end{pmatrix}\begin{pmatrix} -1 & 0 \\ 0 & 1 \end{pmatrix}\begin{pmatrix} \cos\theta & \sin\theta \\ -\sin\theta & \cos\theta \end{pmatrix}$$

$$= \begin{pmatrix} -\cos 2\theta & -\sin 2\theta \\ -\sin 2\theta & \cos 2\theta \end{pmatrix}$$

Without loss of generality, we assume the centroid w is at the origin ($\omega = 0$). Following Appendix I.B, we minimize (1) over θ. Using (3) and noting that $R^t g_i R$ for $i = 0 \; ... \; 2n - 1$ are distance preserving, we minimize the following over θ:

$$\sum_{i=0}^{2n-1}\left\|P_i - \hat{P}_i\right\|^2 = \sum_{i=0}^{2n-1}\left\|R^t g_i^t R P_i - \hat{P}_0\right\|^2$$

Substituting (6), we minimize:

$$\sum_{i=0}^{2n-1}\left\|R^t g_i^t R P_i - \frac{1}{2n}\sum_{j=0}^{2n-1} R^t g_j^t R P_j\right\|^2$$

Rearranging and noting that $R^t g_i^t R = g_i^t$ for $i = 0 \; ... \; n - 1$, we minimize:

$$\sum_{i=0}^{2n-1}\left\|2n R^t g_i^t R P_i - \sum_{j=0}^{n-1} g_j^t P_j - \sum_{j=n}^{2n-1} R_f g_{j-n}^t P_j\right\|^2 \qquad (8)$$

Denote by x_i, y_i the coordinates of the point $g_i^t P_i$ for $i = 0 \; ... \; n - 1$ and $g_{i-n}^t P_i$ for $i = n \; ... \; 2n - 1$. Taking the derivative of (8) with respect to θ we obtain:

$$\tan 2\theta = \frac{\sum_{i=0}^{n-1}\sum_{j=n}^{2n-1}\left(x_i y_j + x_j y_i\right)}{\sum_{i=0}^{n-1}\sum_{j=n}^{2n-1}\left(x_i x_j - y_i y_j\right)} \qquad (9)$$

which is an analytic solution for the case of optimal orientation in 2D. In higher dimensions, however, no analytic solution was found and a minimization procedure is used (except for the mirror symmetry group in 3D where a closed form solution is given (see [35])).

APPENDIX C
DIVIDING POINTS OF A SHAPE INTO SETS

As described in Section III, when measuring C_n-symmetry of a shape represented by a multiple of n points, the points must be divided into sets of n points. In general, this problem is exponential, however when the points are ordered along a contour, as in our case, the possible divisions into sets are more restricted since the ordering is preserved under the symmetry transform of a shape. For example, points in 2D along the contour of a C_n-symmetric shape form orbits which are interlaced. An example is shown in Fig. 29a for C_3-symmetry, where three interlaced orbits are shown marked as •, ○, and □. Thus, given a set of $m = nq$ ordered points there is only one possible division of the points into q sets of n points such that

the ordering is preserved in the symmetric shape—the q sets must be interlaced (as was shown in Fig. 7). In the case of D_n-symmetry (rotational and reflective symmetry of order n) the $m = 2nq$ ordered points, form q orbits which are interlaced and partially inverted to account for the reflection symmetry. An example is shown in Fig. 29b for D_4-symmetry where instead of three interlaced orbits • ○ ☐ • ○ ☐ ... • ○ ☐ • ○ ☐, every other run is inverted: • ○ ☐ ☐ ○ • ... • ○ ☐ ☐ ○ •. Thus, given a set of $m = 2nq$ ordered points there are $m/2n = q$ possible division of the points.
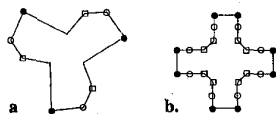

Fig. 29. Dividing m selected points into interlaced sets: a) C_n-symmetry—one possibility; b) D_n-symmetry—$m/2n$ possibilities.

REFERENCES

[1] H. Alt, K. Mehlhorn, H. Wagener, and E. Welzl, "Congruence, similarity, and symmetries of geometric objects," *ACM J. Computing*, vol. 4, pp. 308–315, 1987.

[2] J.L. Amoros, M.J. Buerger, and M. Canut de Amoros, *The Laue Method.* New York: Academic Press, 1975.

[3] M. Atallah, "On symmetry detection," *IEEE Trans. Computers*, vol. 34, no. 7, pp. 663–666, 1985.

[4] F. Attneave, "Symmetry information and memory for patterns," *Am. J. Psychology*, vol. 68, pp. 209–222, 1955

[5] D. Avnir and A.Y. Meyer, "Quantifying the degree of molecular shape deformation. A chirality measure," *J. Molecular Structure (Theochem)*, vol. 94, pp. 211–222, 1991.

[6] J. Bigün, "Recognition of local symmetries in gray value images by harmonic functions," *Proc. Int'l Conf. Pattern Recognition*, pp. 345–347, 1988.

[7] A. Blake, M. Taylor, and A. Cox, "Grasping visual symmetry," *Proc. Int'l Conf. Pattern Recognition*, Berlin, pp. 724–733, May 1993.

[8] H. Blum and R.N. Nagel, "Shape description using weighted symmetric axis features," *Pattern Recognition*, vol. 10, pp. 167–180, 1978.

[9] Y. Bonneh, D. Reisfeld, and Y. Yeshurun, "Texture discrimination by local generalized symmetry," *Proc. Int'l Conf. Pattern Recognition*, pp. 461–465, Berlin, May, 1993.

[10] M. Brady and H. Asada, "Smoothed local symmetries and their implementation," *Int'l J. Robotics Research*, vol. 3, no. 3, pp. 36–61, 1984.

[11] P. Burt and E.H. Adelson, "The Laplacian pyramid as a compact image code," *IEEE Trans. Comm.*, vol. 31, pp. 532–540, 1983.

[12] M.H. DeGroot, "Probability and statistics." Reading, Mass.: Addison-Wesley, 1975.

[13] G. Gilat, "Chiral coefficient—A measure of the amount of structural chirality," *J. Phys. A: Math. Gen.*, vol. 22, p. 545, 1989.

[14] A.D. Gross and T.E. Boult, "Analyzing skewed symmetry," *Int'l J. Computer Vision*, vol. 13, no. 1, pp. 91-111, 1994.

[15] B. Grünbaum, "Measures of symmetry for convex sets," *Proc. Symp. Pure Math: Am. Mathematical Soc.*, vol. 7, pp. 233–270, 1963.

[16] Y. Hel-Or, S. Peleg, and D. Avnir. "Characterization of right handed and left handed shapes," *Computer Vision, Graphics, and Image Processing*, vol. 53, no. 2, 1991.

[17] M-K. Hu, "Visual pattern recognition by moment invariants," *IRE Trans. Information Theory*, vol. 20, pp. 179–187, Feb. 1962.

[18] T. Kanade, "Recovery of the three-dimensional shape of an object from a single view," *Artificial Intelligence*, vol. 17, pp. 409–460, 1981.

[19] M. Kass, A. Witkin, and D. Terzopoulos, "Snakes: Active contour models," *Int'l J. Computer Vision*, vol. 1, pp. 322–332, 1988.

[20] M. Kirby and L. Sirovich, Application of the Karhunen-Loeve procedure for the characterization of human faces," *IEEE Trans. Pattern Analysis and Machine Intelligence*, vol. 12, no. 1, pp. 103–108, 1990.

[21] M. Leyton, *Symmetry, Causality, Mind.* Cambridge, Mass.: MIT Press, 1992.

[22] G. Marola, "On the detection of the axes of symmetry of symmetric and almost symmetric planar images," *IEEE Trans. Pattern Analysis and Machine Intelligence*, vol. 11, no. 1, pp. 104–108, 1989.

[23] W. Miller, *Symmetry Groups And Their Applications.*" London: Academic Press, 1972.

[24] H. Mitsumoto, S. Tamura, K. Okazaki, N. Kajimi, and Y. Fukui, "3D reconstruction using mirror images based on a plane symmetry recovering method," *IEEE Trans. Pattern Analysis and Machine Intelligence*, vol. 14, no. 9, pp. 941-946, 1992.

[25] F. Mokhatarian and A. Mackworth, "A theory of multiscale, curvature-based shape representation for planar curves," *IEEE Trans. Pattern Analysis and Machine Intelligence*, vol. 14, pp. 789–805, 1992.

[26] V.S. Nalwa, "Line-drawing interpretation: Bilateral symmetry," *IEEE Trans. Pattern Analysis and Machine Intelligence*, vol. 11, no. 10, pp. 1,117–1,120, 1989.

[27] W.G. Oh, M. Asada, and S. Tsuji "Model-based matching using skewed symmetry information," *Proc. Int'l Conf. Pattern Recognition*, pp. 1,043–1,045, 1988.

[28] J. Ponce, "On characterizing ribbons and finding skewed symmetries," *Computer Vision, Graphics, and Image Processing*, vol. 52, pp. 328–340, 1990.

[29] D. Reisfeld, H. Wolfson, and Y. Yeshurun "Robust detection of facial features by generalized symmetry," *Proc. Int'l Conf. Pattern Recognition*, Champaign, Ill., pp. 117–120, June 1992.

[30] H. Samet, "The quadtree and related hierarchical data structures," *ACM Computing Surveys*, vol. 16, no. 2, pp. 187–260, June 1984.

[31] D. Terzopoulos, A. Witkin, and M. Kass "Symmetry seeking models and object reconstruction," *Int'l J. Computer Vision*, vol. 1, pp. 211–221, 1987.

[32] H. Weyl, *Symmetry.* Princeton, N.J.: Princeton Univ. Press, 1952.

[33] E. Yodogawa, "Symmetropy, An entropy-like measure of visual symmetry," *Perception and Psychophysics*, vol. 32, no. 3, pp. 230–240, 1982.

[34] H. Zabrodsky, "Computational aspects of pattern characterization—Continuous symmetry," PhD thesis, Hebrew Univ., Jerusalem, Israel, 1993.

[35] H. Zabrodsky and D. Avnir, "Continuous symmetry measures, IV: Chirality," *J. Am. Chemical Soc.*, vol. 117, pp. 462-473, 1995.

[36] H. Zabrodsky and S. Peleg, "Attentive transmission," *J. Visual Comm. and Image Representation*, vol. 1, no. 2, pp. 189–198, Nov. 1990.

[37] H. Zabrodsky, S. Peleg, and D. Avnir, "Continuous symmetry measures II: Symmetry groups and the tetrahedron," *J. Am. Chemical Soc.*, vol. 115, pp. 8,278-8,298, 1993.

[38] H. Zabrodsky, S. Peleg, and D. Avnir, "Symmetry of fuzzy data," *Proc. Int'l Conf. Pattern Recognition*, Tel-Aviv, Israel, pp. 499–504, Oct. 1994.

[39] H. Zabrodsky and D. Weinshall, "3D symmetry from 2D data," *Proc. European Conf. Computer Vision*, Stockholm, Sweden, May 1994.

Hagit Zabrodsky received the BSc degree cum laude in mathematics and computer science in 1985, and the MSc and PhD degrees in computer science in 1989 and 1994, respectively, all from the Hebrew University, Jerusalem, Israel. Dr. Zabrodsky is currently a postdoctoral fellow in the Department of Psychology at Stanford University. Her research interests include computation and human vision, image processing, and visual psychophysics, and she is currently interested in the area of symmetry and color vision.

Shmuel Peleg received his BSc in mathematics from the Hebrew University, Jerusalem, Israel, in 1976, and his MSc and PhD degrees in computer science from the University of Maryland, College Park, in 1978 and 1979, respectively. He has been a faculty member at the Hebrew University of Jerusalem since 1980 and served as chair of the Institute of Computer Science from 1990 to 1992. From 1979 to 1992, he held visiting faculty positions at the University of Maryland, New York University, and the David Sarnoff Research Center. His current research interest is computer vision.

David Avnir is a chemistry professor at the Institute of Chemistry at the Hebrew University, Jerusalem, Israel. He joined the university faculty in 1980 and was appointed chair of the School of Chemistry in 1991, holding that position for three years. In 1992, he was appointed founding editor and editor-in-chief of *Heterogeneous Chemistry Reviews*. His scientific activities include sol-gel materials, fractal theory and its applications in surface science and catalysis, surface photophysics, far-from-equilibrium phenomena, and symmetry and chirality in chemistry. He has authored more than 170 scientific papers on these topics and edited the highly cited book, *The Factual approach to Heterogeneous Chemistry*. He has been a member of numerous scientific committees and is on the editorial boards of *Chemistry of Materials, Journal of Sol-Gel Science and Technology*, and *the International Journal of Discrete Chaotic Dynamics*. He was the recipient of the E.D. Bergmann Award for Distinction in Research.